Giant resonances in ^{40}Ca and ^{48}Ca

M. R. Anders,[1] S. Shlomo,[1] Tapas Sil,[1,2] D. H. Youngblood,[1] Y.-W. Lui,[1] and Krishichayan[1,3]
[1]*Cyclotron Institute, Texas A&M University, College Station, Texas 77843, USA*
[2]*Indian Institute of Information Technology Design and Manufacturing, Kancheepuram, Chennai 600 127, Tamil Nadu, India*
[3]*Department of Pure and Applied Physics, Guru Ghasidas University, Bilaspur-495009 C G, India*
(Received 30 November 2012; published 6 February 2013)

We present results of fully self-consistent Hartree-Fock-based random phase approximation calculations of the strength functions $S(E)$ and centroid energies $E_{\rm CEN}$ of isoscalar ($T = 0$) and isovector ($T = 1$) giant resonances of multipolarities $L = 0$–3 in ^{40}Ca and ^{48}Ca, using a wide range of commonly employed 18 Skyrme-type nucleon-nucleon effective interactions. We determined the sensitivities of $E_{\rm CEN}$ and of the isotopic differences $E_{\rm CEN}(^{48}{\rm Ca}) - E_{\rm CEN}(^{40}{\rm Ca})$ to physical quantities, such as nuclear matter incompressibility coefficient, symmetry energy density, and effective mass, associated with the Skyrme interactions and compare the results with the available experimental data.

DOI: 10.1103/PhysRevC.87.024303 PACS number(s): 24.30.Cz, 21.60.Jz, 21.65.−f, 27.40.+z

I. INTRODUCTION

The study of collective modes in nuclei was the subject of extensive theoretical and experimental studies during several decades [1–3] because it contributes significantly to our understanding of bulk properties of nuclei, their nonequilibrium properties, and properties of the nuclear force. Of particular interest is the equation of state (EOS), i.e., the binding energy per nucleon as a function of the neutron (N) and proton (Z) densities, of infinite nuclear matter (no Coulomb interaction). The EOS is an important ingredient in the study of properties of nuclei at and away from stability, the study of structure, and evolution of compact astrophysical objects, such as neutron stars and core-collapse supernovae, and the study of heavy-ion collisions (HIC) [4,5]. The saturation point of the equation of state for symmetric ($N = Z$) nuclear matter (NM) is well determined from the measured binding energies and central matter densities of nuclei, by extrapolation to infinite NM [1,2]. To extend our knowledge of the EOS beyond the saturation point of symmetric NM, an accurate value of the NM incompressibility coefficient $K_{\rm NM}$, which is directly related to the curvature of the EOS of symmetric NM, is needed. An accurate knowledge of the dependence of the symmetry energy, $E_{\rm sym}(\rho)$, on the matter density ρ is needed for the EOS of asymmetric NM.

There have been many attempts over the years to determine $K_{\rm NM}$ and $E_{\rm sym}(\rho)$ by considering physical quantities which are sensitive to the values of $K_{\rm NM}$ and $E_{\rm sym}(\rho)$ [3,4,6,7]. In this work we investigate the sensitivity of the strength function distributions of the isoscalar and isovector giant resonances with multipolarities $L = 0$–3 of the isotopes ^{40}Ca and ^{48}Ca to bulk properties of NM, such as $K_{\rm NM}$, $E_{\rm sym}$, and the effective mass m^*. It is well known that the energies of the compression modes, the isoscalar giant monopole resonance (ISGMR), and isoscalar giant dipole resonance (ISGDR), are very sensitive to the value of $K_{\rm NM}$ [1,3,8]. Also the energies of the isovector giant resonances, in particular, the isovector giant dipole resonance (IVGDR), are sensitive to the density dependence of $E_{\rm sym}$ [9,10], commonly parametrized in terms of the quantities J, L, and $K_{\rm sym}$, which are the value of $E_{\rm sym}(\rho)$ at saturation density (also known as symmetry energy coefficient), and the quantities directly related to the derivative and the curvature of $E_{\rm sym}(\rho)$ at the saturation density, respectively. Furthermore, information on the density dependence of $E_{\rm sym}$ can also be obtained by studying the isotopic dependence of strength functions, such as the difference between the strength functions of ^{40}Ca and ^{48}Ca and between ^{112}Sn and ^{124}Sn. We note that the value of the neutron-proton asymmetry parameter $\delta = (N - Z)/A$ increases from ^{40}Ca to ^{48}Ca by a value of 0.167 which is significantly larger than the change of 0.087 between ^{112}Sn and ^{124}Sn.

In early analysis of the experimental data on the ISGMR [11,12], a semiclassical model was adopted to relate the energy of the ISGMR to an incompressibility coefficient $K_{\rm A}$ of the nucleus and carry out a Leptodermous ($A^{-1/3}$) expansion of $K_{\rm A}$, similar to a mass formula, to parameterize $K_{\rm A}$ into volume ($K_{\rm NM}$), surface ($K_{\rm S}$), symmetry (K_τ), and Coulomb ($K_{\rm C}$) terms [11,13,14]. Shlomo and Youngblood [14] showed that this type of analysis could not provide a unique solution even including all available world data as of that time. More recently [15] a semiclassical analysis of the ISGMR data in the Sn isotopes demonstrated that the value obtained for K_τ is quite sensitive to the number of terms employed in the Leptodermous expansion. In this work we adopt the microscopic approach of fully self-consistent Hartree-Fock (HF)-based random phase approximation (RPA), employing an effective nucleon-nucleon interaction. In the HF-RPA approach, the values of $K_{\rm NM}$ and the density dependence of $E_{\rm sym}$ are then deduced from the interaction that best reproduces the experimental data on the strength functions of the giant resonance (see the review in Ref. [3]). It is important to note that ground-state properties of nuclei are well described by the HF approximation, using an effective nucleon-nucleon interaction, such as the Skyrme-type interaction [16–18], with parameters obtained by a fit to a selected set of experimental data on binding energies and radii of nuclei [1,2]. It was also demonstrated that HF-based RPA nicely reproduces the properties of low-lying collective states as well as of giant resonances [1,2].

TABLE I. Values for the parameters for the following Skyrme interactions: SGII [23], KDE0 [24], KDE0v1 [24], SKM* [25], SK255 [26], SkI3 [40], SkI4 [40], SkI5 [40], SV-bas [41], SV-min [41], SV-m56-O [42], SV-m64-O [42], SLy4 [43], SLy5 [43], SLy6 [43], SkMP [44], SkP [45], and SkO' [46]. These parameters are given in the following units: t_0 (MeV fm^3), t_1 (MeV fm^5), t_2 (MeV fm^5), t_3 (MeV fm$^{3(\alpha+1)}$), W_0 (MeV), and the remaining parameters are dimensionless.

Force	t_0	t_1	t_2	t_3	W_0	x_0	x_1	x_2	x_3	X_w	α
SGII	−2645.00	340.00	−41.90	15595.00	105.00	0.0900	−0.0588	1.4250	0.0604	1.0000	1/6
KDE0	−2526.51	430.94	−398.38	14235.52	128.96	0.7583	−0.3087	−0.9495	1.1445	1.0000	0.1676
KDE0v1	−2553.08	411.70	−419.87	14603.61	124.41	0.6483	−0.3472	−0.9268	0.9475	1.0000	0.1673
SKM*	−2645.00	410.00	−135.00	15595.00	130.00	0.0900	0.0000	0.0000	0.0000	1.0000	1/6
SK255	−1689.35	389.30	−126.07	10989.60	95.39	−0.1461	0.1660	0.0012	−0.7449	1.0000	0.3563
SkI3	−1762.88	561.61	−227.09	8106.20	188.51	0.3083	−1.1722	−1.0907	1.2926	0.0000	1/4
SkI4	−1885.83	473.83	1006.86	9703.61	366.19	0.4051	−2.8891	−1.3252	1.1452	−0.9850	1/4
SkI5	−1772.91	550.84	−126.69	8206.25	123.63	−0.1171	−1.3088	−1.0487	0.3410	1.0000	1/4
SV-bas	−1879.64	313.75	112.68	12527.38	124.63	0.2585	−0.3817	−2.8236	0.1232	0.5474	0.3000
SV-min	−2112.25	295.78	142.27	13988.57	111.29	0.2439	−1.4349	−2.6259	0.2581	0.8255	0.2554
SV-m56-O	−1905.40	571.19	1594.80	8439.04	133.27	0.6440	−2.9737	−1.2553	1.7966	0.7949	0.2000
SV-m64-O	−2083.86	484.60	1134.35	10720.67	113.97	0.6198	−2.3327	−1.3059	1.2101	1.1042	0.2000
SLy4	−2488.91	486.82	−546.39	13777.00	123.00	0.8340	−0.3440	−1.0000	1.3540	1.0000	1/6
SLy5	−2484.88	483.13	−549.40	13763.00	126.00	0.7780	−0.3280	−1.0000	1.2670	1.0000	1/6
SLy6	−2479.50	462.18	−448.61	13673.00	122.00	0.8250	−0.4650	−1.0000	1.3550	1.0000	1/6
SkMP	−2372.24	503.62	57.28	12585.30	160.00	−0.1576	−0.4029	−2.9557	−0.2679	1.0000	1/6
SkP	−2931.70	320.62	−337.41	18708.97	100.00	0.2922	0.6532	−0.5373	0.1810	1.0000	1/6
SkO'	−2099.42	301.53	154.78	13526.46	287.79	−0.0295	−1.3257	−2.3234	−0.1474	−0.5760	1/4

Recently the giant resonance region from 9.5 MeV $< E_x <$ 40 MeV in ^{48}Ca was studied with inelastic scattering of 240 MeV α particles at small angles, including 0°. Close to 100% of the ISGMR ($E0$), ISGDR ($E1$), and isoscalar giant quadrupole resonance ($E2$) strengths have been located between 9.5 and 40 MeV in ^{48}Ca [19]. To study the effect of neutron-proton asymmetry, a comparison with the available data for ^{40}Ca [20–22], as well as with the results obtained within the HF-based RPA, was carried out in Ref. [19]. The ISGMR was found at somewhat higher energy in ^{48}Ca than in ^{40}Ca, whereas self-consistent HF-RPA calculations obtained using the SGII [23], KDE0 [24], SKM* [25], and SK255 [26] Skyrme interactions predict a centroid energy in this neutron-rich Ca isotope lower than in ^{40}Ca.

In this work we extend our theoretical investigation by considering the isoscalar and isovector giant resonances of multipolarities $L = 0$–3 in ^{40}Ca and ^{48}Ca. In the next section we review the basic elements of the self-consistent HF-based RPA theory for the strength functions of isoscalar ($T = 0$) and isovector ($T = 1$) giant resonances. In Sec. III we present results of our calculations for the strength functions $S(E)$ and centroid energies $E_{\rm CEN}$ obtained for giant resonances of $T = 0$, 1 and multipolarities $L = 0$–3 in ^{40}Ca and ^{48}Ca, using a wide range of 18 commonly used Skyrme-type nucleon-nucleon effective interactions. We pay attention to the issue of self-consistency and investigate the sensitivities of $E_{\rm CEN}$ and of the isotopic differences $E_{\rm CEN}(^{48}{\rm Ca}) - E_{\rm CEN}(^{40}{\rm Ca})$ to physical quantities, such as nuclear matter incompressibility coefficient, symmetry energy density and effective mass, associated with the effective nucleon-nucleon interactions, and compare the results with available experimental data. In the last section, we discuss our results and present our conclusions.

TABLE II. Same as Table I with the following conditions defining the interactions: HBTM, for proton and neutron $\hbar^2/2m = 20.7525$ MeV fm^2 for 0, for proton $\hbar^2/2m = 20.7213$ MeV fm^2, and neutron $\hbar^2/2m = 20.7498$ MeV fm^2 for 1, and for proton and neutron $\hbar^2/2m = 20.7355$ MeV fm^2 for 2; JTM, contribution to the spin-orbit potential from t_1 and t_2 is taken for 1 and not for 0; CEX, Coulomb exchange on for 1 and off for 0; RHOC, proton density is used for Coulomb potential for 0 and charge density is used for Coulomb potential for 1; ZPE, center-of-mass correction is taken as (1-1/A) factor on the mass for 1 and is computed explicitly *a posteriori* as $E_{\rm c.m.} = \frac{1}{2mA}\langle \hat{P}^2 \rangle$ for 0.

Force	Ref.	HBTM	JTM	CEX	RHOC	ZPE
SGII	[23]	0	0	1	0	0
KDE0	[24]	2	1	0	0	1
KDE0v1	[24]	2	1	0	0	1
SKM*	[25]	0	0	1	0	0
SK255	[26]	2	1	0	0	1
SkI3	[40]	0	0	1	0	1
SkI4	[40]	0	0	1	0	1
SkI5	[40]	0	0	1	0	1
SV-bas	[41]	1	0	1	0	1
SV-min	[41]	1	0	1	0	1
SV-m56-O	[42]	1	0	1	0	1
SV-m64-O	[42]	1	0	1	0	1
SLy4	[43]	2	0	1	0	0
SLy5	[43]	2	1	1	0	0
SLy6	[43]	2	0	1	0	1
SkMP	[44]	0	0	1	0	0
SkP	[45]	2	1	1	0	0
SkO'	[46]	2	1	1	0	1

II. SELF-CONSISTENT HF-BASED RPA APPROACH

In numerical calculations of the properties of giant resonances in nuclei within the HF-based RPA theory, one starts by adopting an effective nucleon-nucleon interaction V_{12}, such as the Skyrme interaction, with parameters determined by a fit of the HF predictions to experimental data on ground-state

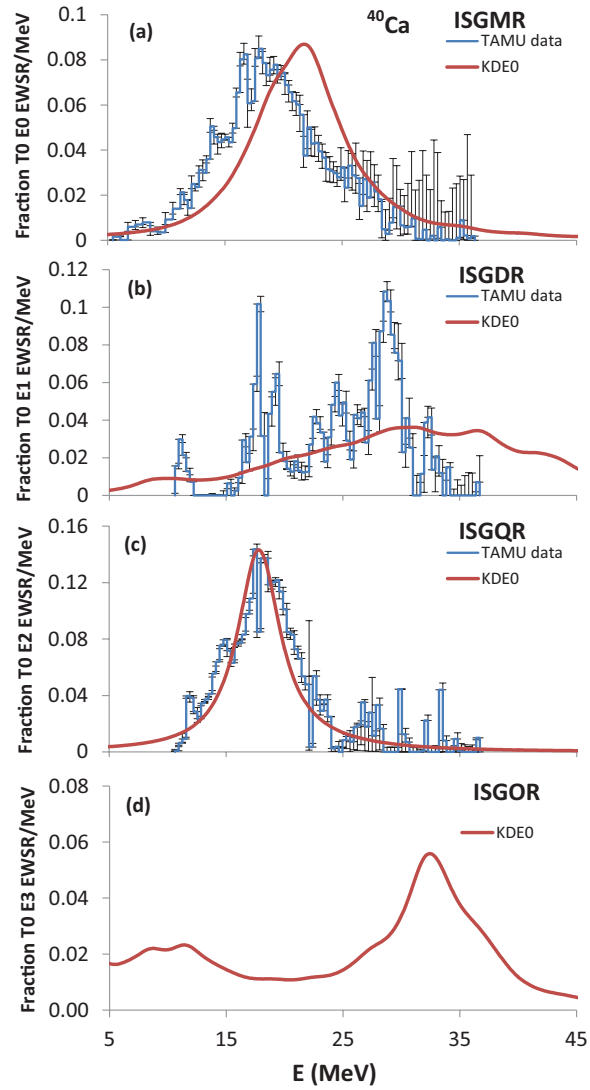

FIG. 1. (Color online) Self-consistent HF-based RPA results (solid lines) for the distribution of the energy-weighted strength, normalized to one (fraction of EWSR), for the isoscalar monopole ($E0$), dipole ($E1$), quadrupole ($E2$), and octopole ($E3$) in ^{40}Ca, obtained using the KDE0 [24] Skyrme interaction. For the purpose of comparison with experiment a Lorenzian smearing of a 3 MeV width was used in the calculation. The experimental data [21] are shown as histograms.

properties, such as binding energies and radii, of a selected set of a wide range of nuclei. Then, the RPA equations are solved using the particle-hole interaction deduced from V_{12}, by employing a certain numerical method [27–29], and the physical quantities of interest, such as the strength functions $S(E)$ and transition densities, are calculated. We point out that in a fully self-consistent HF-based RPA calculation, one should include all the components of V_{12} in the RPA calculations and use a sufficiently large particle-hole configuration space to insure convergence. Necessary conditions for fully self-consistent calculations are as follows: (i) The spurious isoscalar dipole state (due to center-of-mass motion) is obtained at zero energy; and (ii) the energy weighted sun rules (EWSR) are fulfilled.

A. Skyrme energy density functional

In our calculations we have adopted the following form for the Skyrme-type effective nucleon-nucleon interaction [30]:

$$
\begin{aligned}
V_{12} = {} & t_0\left(1+x_0P_{12}^{\sigma}\right)\delta(\vec{r}_1-\vec{r}_2)+\frac{1}{2}t_1\left(1+x_1P_{12}^{\sigma}\right)\\
& \times\left[\overleftarrow{k}_{12}^{2}\delta(\vec{r}_1-\vec{r}_2)+\delta(\vec{r}_1-\vec{r}_2)\vec{k}_{12}^{2}\right]\\
& +t_2\left(1+x_2P_{12}^{\sigma}\right)\overleftarrow{k}_{12}\delta(\vec{r}_1-\vec{r}_2)\vec{k}_{12}\\
& +\frac{1}{6}t_3\left(1+x_3P_{12}^{\sigma}\right)\rho^{\alpha}\left(\frac{\vec{r}_1+\vec{r}_2}{2}\right)\delta(\vec{r}_1-\vec{r}_2)\\
& +iW_0\overleftarrow{k}_{12}\delta(\vec{r}_1-\vec{r}_2)(\vec{\sigma}_1+\vec{\sigma}_2)\times\vec{k}_{12}, \qquad (1)
\end{aligned}
$$

where t_i, x_i, α, and W_0 are the parameters of the interaction and P_{12}^{σ} is the spin exchange operator, $\vec{\sigma}_i$ is the Pauli spin operator, $\vec{k}_{12}=-i(\vec{\nabla}_1-\vec{\nabla}_2)/2$, and $\overleftarrow{k}_{12}=-i(\overleftarrow{\nabla}_1-\overleftarrow{\nabla}_2)/2$. Here, the right and left arrows indicate that the momentum operators act

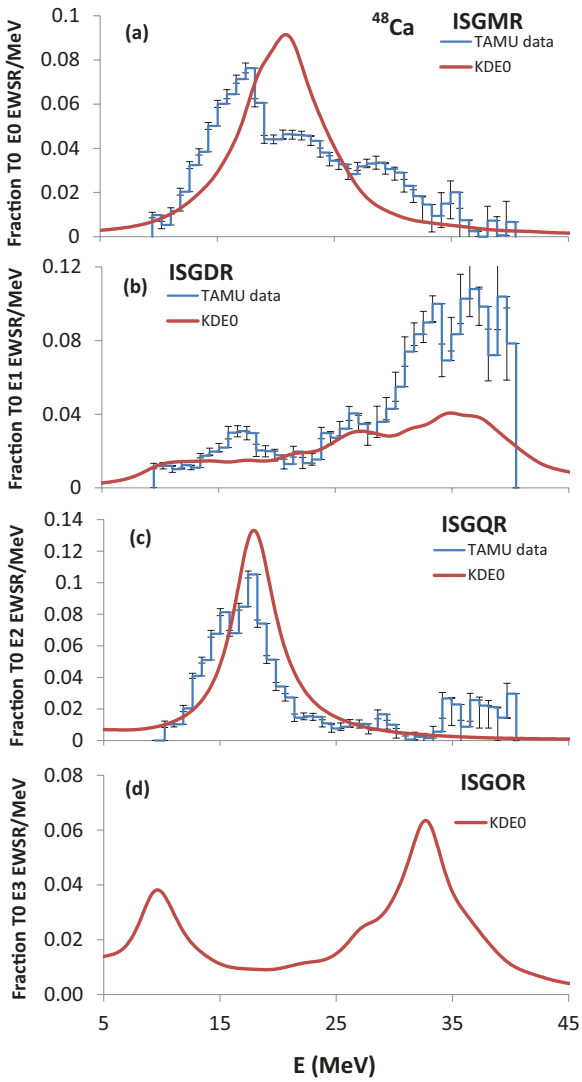

FIG. 2. (Color online) Same as Fig. 1 except for ^{48}Ca. Experimental data is from Ref. [19].

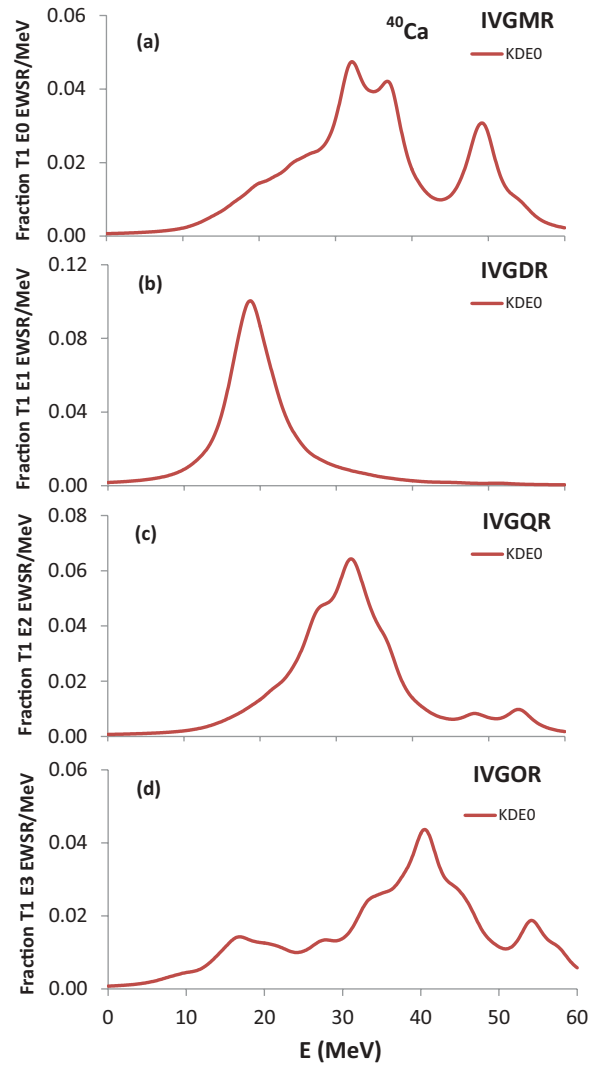

FIG. 3. (Color online) Self-consistent HF-based RPA results (solid lines) for the distribution of the energy-weighted strength, normalized to one (fraction of EWSR), for the isovector monopole ($E0$), dipole ($E1$), quadrupole ($E2$), and octopole ($E3$) in ^{40}Ca, obtained using the KDE0 [24] Skyrme interaction. A Lorenzian smearing of a 3 MeV width was used in the calculation.

on the right and on the left, respectively. The corresponding mean-field $V_{\rm HF}$ and the total energy E of the system are given by

$$V_{\rm HF} = \frac{\delta H}{\delta \rho}, \quad E = \int H(r)\, d^3r, \tag{2}$$

respectively, where $H(r)$ is the Skyrme energy-density functional, [31] obtained using Eq. (1). It is given by [30]

$$H = K + H_0 + H_3 + H_{\rm eff} + H_{\rm fin} + H_{\rm so} + H_{\rm sg} + H_{\rm Coul}, \tag{3}$$

where,

$$K = \frac{\hbar^2}{2m}\tau, \tag{4}$$

is the kinetic-energy term. For the Skyrme interaction of Eq. (1), we have

$$H_0 = \tfrac{1}{4}t_0\left[(2+x_0)\,\rho^2 - (2x_0+1)\left(\rho_p^2+\rho_n^2\right)\right], \tag{5}$$

$$H_3 = \tfrac{1}{24}t_3\rho^\alpha\left[(2+x_3)\,\rho^2 - (2x_3+1)\left(\rho_p^2+\rho_n^2\right)\right], \tag{6}$$

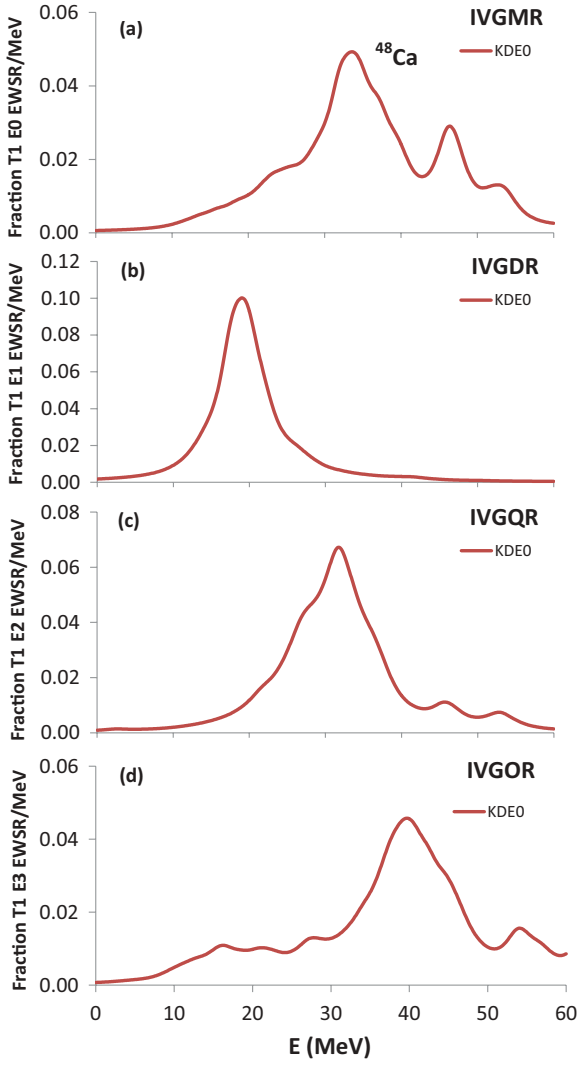

FIG. 4. (Color online) Same as Fig. 3 except for ^{48}Ca.

$$H_{\rm eff} = \tfrac{1}{8}\left[t_1(2+x_1) + t_2(2+x_2)\right]\tau\rho + \tfrac{1}{8}\left[t_2(2x_2+1) - t_1(2x_1+1)\right](\tau_p\rho_p + \tau_n\rho_n), \tag{7}$$

$$H_{\rm fin} = \tfrac{1}{32}\left[3t_1(2+x_1) - t_2(2+x_2)\right](\nabla\rho)^2 - \tfrac{1}{32}\left[3t_1(2x_1+1) + t_2(2x_2+1)\right]\left[(\nabla\rho_p)^2 + (\nabla\rho_n)^2\right], \tag{8}$$

$$H_{\rm so} = \frac{W_0}{2}[J\cdot\nabla\rho + x_w(J_p\cdot\nabla\rho_p + J_n\cdot\nabla\rho_n)], \tag{9}$$

and

$$H_{\rm sg} = -\tfrac{1}{16}(t_1x_1 + t_2x_2)\,J^2 + \tfrac{1}{16}(t_1 - t_2)\left(J_p^2 + J_n^2\right). \tag{10}$$

Here, H_0 is the zero-range term, H_3 is the density-dependent term, $H_{\rm eff}$ is an effective-mass term, $H_{\rm fin}$ is a finite-range term, $H_{\rm so}$ is a spin-orbit term, $H_{\rm sg}$ is a term that is due

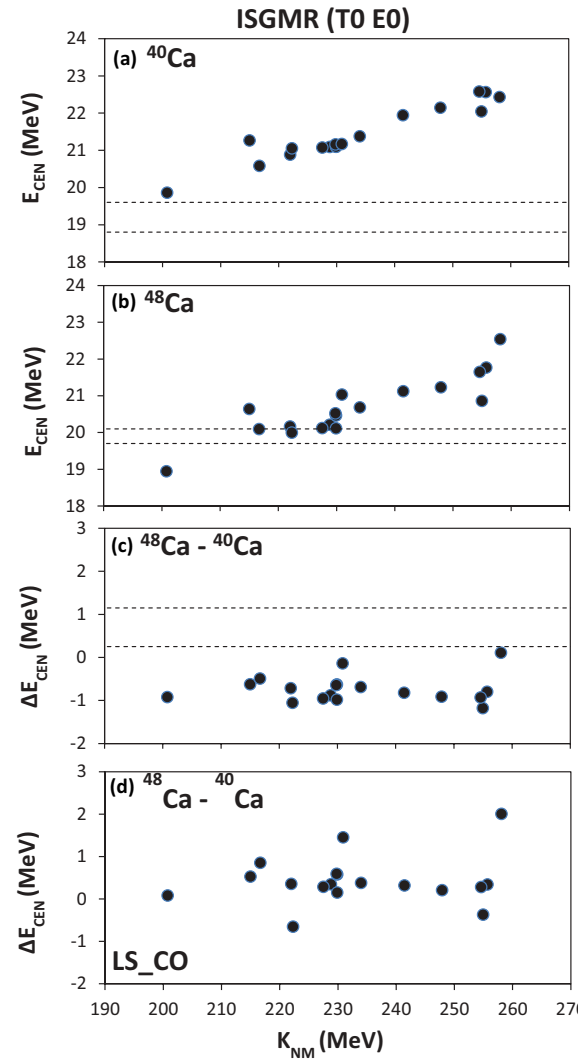

FIG. 5. (Color online) Comparison of experimental data [19,21] of the ISGMR centroid energies of ^{40}Ca (a), ^{48}Ca (b), and the ^{48}Ca –^{40}Ca energy difference (c), shown as the regions between the dashed lines, with the results of fully self-consistent HF-based RPA calculations (solid circles) obtained using the Skyrme interactions of Table I, plotted vs. $K_{\rm NM}$. The results obtained with violation of self-consistency in the RPA calculations are shown in (d).

to tensor coupling with spin and gradient and $H_{\rm Coul}$ is the contribution to the energy density that is due to the Coulomb interaction. In Eqs. (5)–(10) $\rho = \rho_p + \rho_n$, $\tau = \tau_p + \tau_n$, and $J = J_p + J_n$, are the particle number density, kinetic-energy density, and spin-density with p and n denoting the protons and neutrons, respectively [30]. Note that the additional parameter x_w, introduced in Eq. (9), allows us to modify the isospin dependence of the spin-orbit term.

The contribution to the energy-density, Eq. (3), from the Coulomb interaction can be written as a sum of a direct and an exchange term:

$$H_{\rm Coul}(r) = H^{\rm dir}_{\rm Coul}(r) + H^{\rm ex}_{\rm Coul}(r). \tag{11}$$

For the direct term it is common to adopt the expression,

$$H^{\rm dir}_{\rm Coul}(r) = \frac{1}{2}e^2\rho_p(r)\int\frac{\rho_p(r')}{|r-r'|}d^3r', \tag{12}$$

and for the corresponding exchange term to use the Slater approximation,

$$H^{\rm ex}_{\rm Coul}(r) = -\frac{3}{4}e^2\rho_p(r)\left[\frac{3\rho_p(r)}{\pi}\right]^{1/3}. \tag{13}$$

It is very important to emphasize that the definitions of Eqs. (12) and (13) are not for the *bona fide* direct and exchange terms because each of them includes the contributions of the self-interaction term, which appear in opposite signs and cancel out in Eq. (11); see Ref. [32].

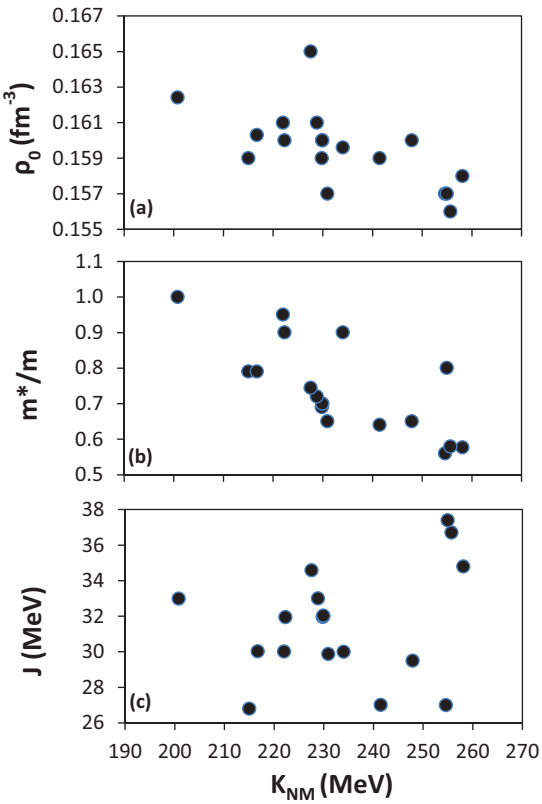

FIG. 6. (Color online) The values of ρ_0, m^*/m, and J are plotted vs $K_{\rm NM,}$ for the Skyrme interactions of Table I.

The HF approach applied to finite nuclei violates translational invariance, introducing a spurious center-of-mass (c.m.) motion. Thus, one must extract the contributions of the c.m. motion to the binding energy B, rms radii, and other observables. To account for the c.m. correction to the total binding energy, one must subtract from it the so-called c.m. energy given as

$$E_{\rm c.m.} = \frac{1}{2mA}\langle\hat{P}^2\rangle, \tag{14}$$

where, $P = -i\hbar\sum_i \nabla_i$ is the total linear momentum operator.

During the last four decades, many Skyrme type effective nucleon-nucleon interactions of different forms were obtained by fitting the HF results to selected sets of experimental data [33,34]. We emphasize that in this work we consider the specific form of Eq. (1) for the Skyrme-type interaction. The values of the Skyrme parameters of the interactions adopted in this work are listed in Table I. It is very important to note that in determining the parameters of the Skyrme interaction, Eq. (1), several approximations, concerning the terms of Eqs. (4), (10), (11), and (14), were made in the HF calculations. These approximations, which should be taken into account for a proper application of the specific interaction

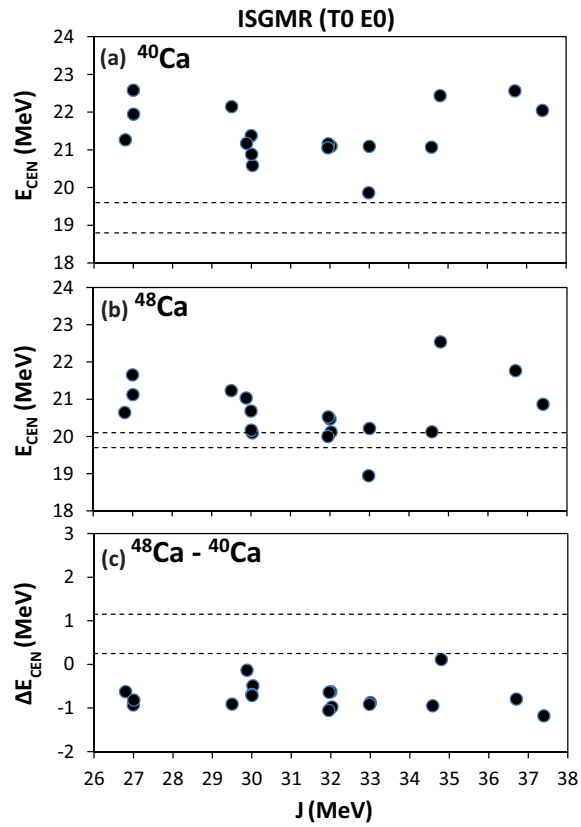

FIG. 7. (Color online) The HF-based RPA results (solid circles) of the ISGMR centroid energies $E_{\rm CEN}$ of ^{40}Ca (a), ^{48}Ca (b), and the ^{48}Ca–^{40}Ca energy difference (c), obtained using the Skyrme-type interactions of Table I, as a function of the NM symmetry energy at saturation density J. The limits on the experimental data are shown by the dashed lines.

in fully self-consistent HF-based RPA calculations, are

(i) *The kinetic term, Eq.* (4). In some interactions the mass of the proton is taken to be equal to that of the neutron and a certain value for the nucleon mass is adopted. In other interactions the mass of the proton is taken to be different than that of the neutron.

(ii) *The spin-density terms, Eq.* (10). In some interactions the contributions from the spin-density term as given by Eq. (10), are ignored. We note that contributions from Eq. (10) are crucial for the calculation of the Landau parameter G_0'.

(iii) *The Coulomb term, Eq.* (11). In some interactions the Coulomb term of Eq. (13) is omitted. It is important to note that by neglecting the term of Eq. (13), one neglects the *bona fide* Coulomb exchange term together with the spurious contribution of the self-interaction term. This leads to a contribution to Coulomb displacement energies, obtained from Eq. (12), which is in better agreement with experimental data [35], because in the HF calculations with Skyrme interactions one neglects the contributions due to charge symmetry breaking in the nucleon-nucleon interaction and the contribution to Coulomb energy associated with long-range correlations. Also, in some interactions the charge density is used in Eq. (11), instead of the point proton density.

(iv) *The center of mass correction, Eq.* (14). Traditionally, one simplifies the computation of Eq. (14) by taking into account only the one-body parts of it, which can be easily achieved by replacing $\frac{1}{m} \rightarrow \frac{1}{m}[1 - \frac{1}{A}]$ in the kinetic-energy term. In this case, the effects of neglecting the two-body part of Eq. (14) are compensated by renormalization of the force parameters. This may induce in the forces an incorrect trend with respect to the nucleon number A that becomes visible in the nuclear matter properties. A more appropriate approach, used in some interactions, is to take into account the contribution of the two body terms by using the HF single-particle wave functions or by employing a simple scheme to evaluate Eq. (14).

The approximations that were used to obtain the Skyrme interactions adopted in this work are listed for each interaction in Table II.

B. RPA calculations of strength functions

In this work we have carried out fully self-consistent HF-based RPA calculations for electric giant resonances in ^{40}Ca and ^{48}Ca using the effective energy density functionals (EDF) given by Eqs. (3)–(14) with Tables I and II and employing the numerical method for RPA described in Refs. [28,36,37], which is formulated in terms of coordinatelike Q (time-even) and momentumlike P (time-odd) particle-hole (p-h) operators and adapted for a given EDF. We point out that to insure self-consistency we have carried out the calculations using a large p-h space and included all the terms of the p-h residual interaction (time-even and time-odd) which are associated with the EDF used in the HF calculations. No additional time-odd residual interactions were added. For a given scattering

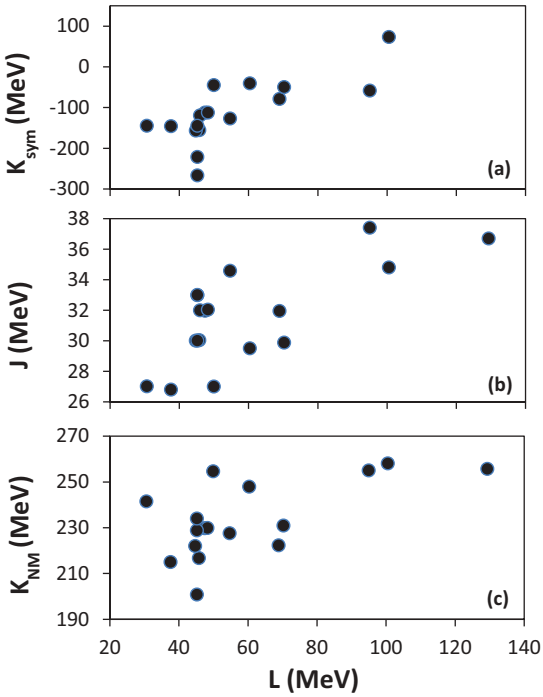

FIG. 8. (Color online) The values of $K_{\rm sym}$, J, and $K_{\rm NM}$ are plotted vs L, for the Skyrme interactions of Table I.

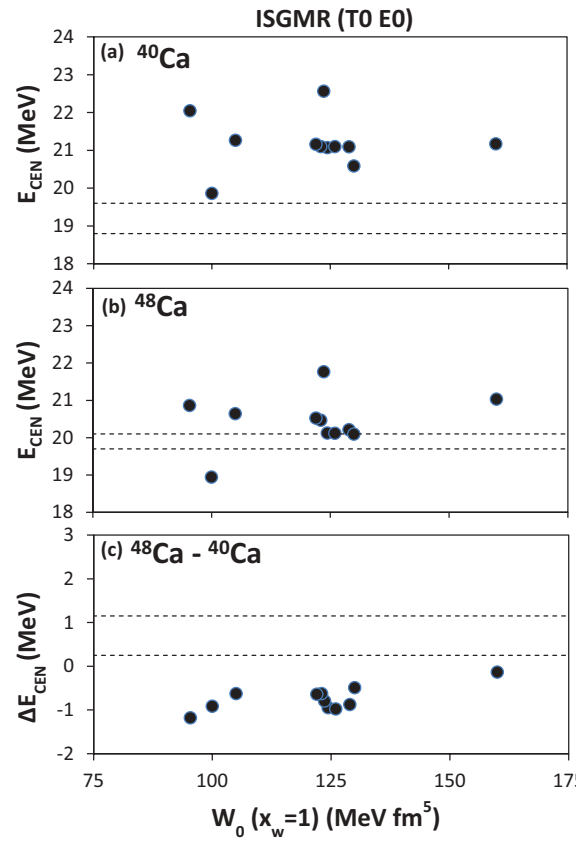

FIG. 9. (Color online) Same as Fig. 7 except as a function of the strength W_0 of the spin-orbit interaction.

operator F_L, we have calculated the strength function,

$$S(E) = \sum_j |\langle 0|F_L|j\rangle|^2 \delta(E_j - E_0). \quad (15)$$

Here, $|0\rangle$ is the RPA ground state and the sum is over all RPA excited states $|j\rangle$ with the corresponding excitation energies E_j. We adopt the single-particle scattering operator,

$$F_L = \sum_i f(r_i) Y_{L0}(i), \quad (16)$$

for isocalar ($T = 0$) excitations and

$$F_L = \frac{Z}{A} \sum_n f(r_n) Y_{L0}(n) - \frac{N}{A} \sum_p f(r_p) Y_{L0}(p), \quad (17)$$

for isovector excitations ($T = 1$). In Eqs. (16) and (17) we use the operator $f(r) = r$, for the isovector dipole ($T = 1$, $L = 1$) and $f(r) = r^3 - (5/3)\langle r^2\rangle r$ for the isoscalar dipole ($T = 0$, $L = 1$), to eliminate possible contribution of the spurious state mixing [38,39]. For the isoscalar and isovector monopole ($L = 0$), quadrupole ($L = 2$), and octopole ($L = 3$) excitations we use the operators r^2, r^2, and r^3, respectively. We then determine the energy moments of the strength function,

$$m_k = \int_0^\infty E^k S(E) dE. \quad (18)$$

The centroid energy, $E_{\rm CEN}$, is then obtained from

$$E_{\rm CEN} = \frac{m_1}{m_0}. \quad (19)$$

The energy moment m_1 can also be calculated using the HF ground-state wave function, thereby leading to an energy weighted sum rule (EWSR) [1,10]. For the isoscalar F_L in Eq. (16), the EWSR is given by

$$m_1(L, T = 0) = \frac{1}{4\pi} \frac{\hbar^2}{2m} \int g_L(r) \rho(r) 4\pi r^2 dr, \quad (20)$$

where $\rho(r)$ is the HF ground-state matter density distribution and

$$g_L(r) = \left(\frac{df}{dr}\right)^2 + L(L+1)\left(\frac{f}{r}\right)^2. \quad (21)$$

For the isovector ($T = 1$) operator F_L of Eq. (17), the EWSR is given by

$$m_1(L, T = 1) = \frac{NZ}{A^2} m_1(L, T = 0)[1 + \kappa - \kappa_{np}], \quad (22)$$

where κ is the enhancement factor which is due to the momentum dependence of the effective nucleon-nucleon interaction and is given by

$$\kappa = \frac{(1/2)[t_1(1 + x_1/2) + t_2(1 + x_2/2)]}{(\hbar^2/2m)(4NZ/A^2)} \times \frac{2\int g_L(r)\rho_p(r)\rho_n(r)4\pi r^2 dr}{\int g_L(r)\rho(r)4\pi r^2 dr}, \quad (23)$$

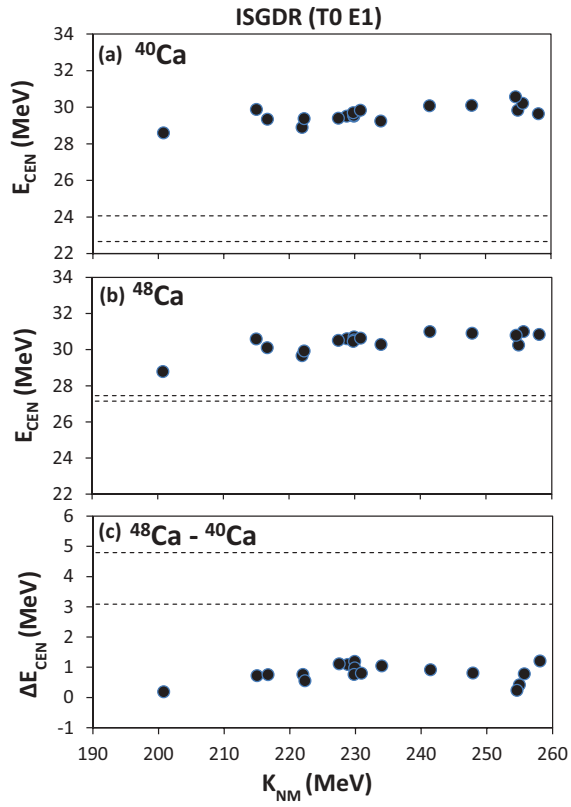

FIG. 10. (Color online) Same as Fig. 7 except for the ISGDR as a function of $K_{\rm NM}$.

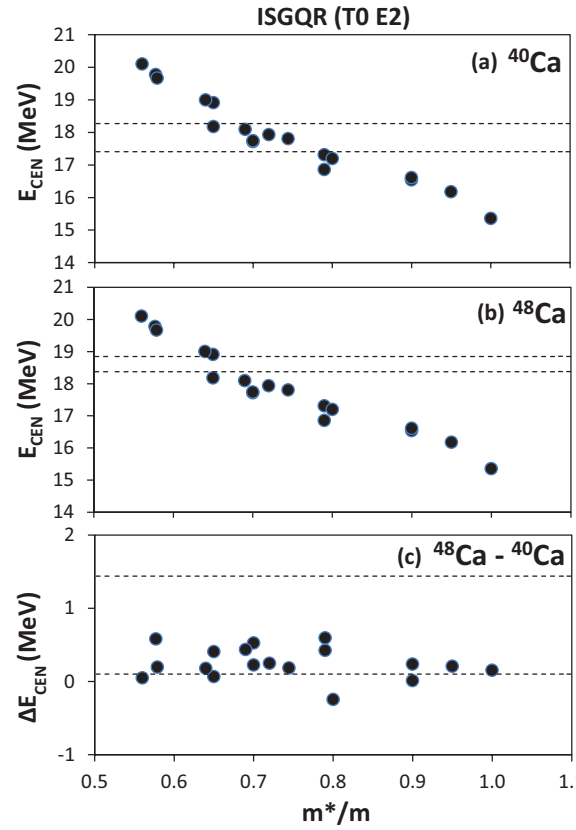

FIG. 11. (Color online) Same as Fig. 7 except for the ISGQR as a function of m^*/m.

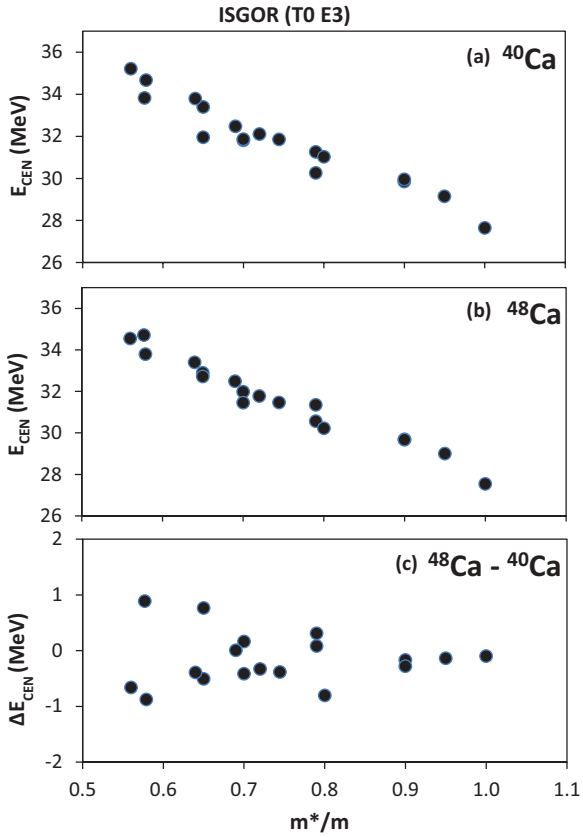

FIG. 12. (Color online) Same as Fig. 11 except for the ISGOR.

where t_i and x_i are the parameters of the Skyrme interaction. The correction κ_{np}, which arises because of the difference in the profiles of the neutron and proton density distributions [i.e., because $\rho_n(r) - \rho_p(r) \neq \frac{N-Z}{A}\rho(r)$], is given by

$$\kappa_{np} = \frac{(N-Z)}{A}\frac{A}{NZ}\frac{\int g_L(r)[Z\rho_n(r) - N\rho_p(r)]4\pi r^2 dr}{\int g_L(r)\rho(r)4\pi r^2 dr}. \tag{24}$$

We have carried out fully self-consistent Hartree-Fock-based RPA calculations of the isoscalar giant monopole resonance (ISGMR), dipole (ISGDR), quadrupole (ISGQR), and the octopole (ISGOR) strength functions, adopting the scattering operator of Eq. (16), and for the isovector giant monopole resonance (IVGMR), dipole (IVGDR), quadrupole (IVGQR), and octopole (IVGOR) strength functions, adopting the scattering operator of Eq. (17), for ^{40}Ca and for ^{48}Ca, using a wide range of 18 Skyrme-type effective interactions (Table I). In the next section we present the results of our calculations and compare with available experimental data.

C. Equation of state of nuclear matter

In the vicinity of the saturation density ρ_0 of symmetric NM, the EOS can be approximated by

$$E_0[\rho] = E[\rho_0] + \frac{1}{18}K_{\rm NM}\left(\frac{\rho-\rho_0}{\rho_0}\right)^2, \tag{25}$$

where $E_0[\rho]$ is the binding energy per nucleon and $K_{\rm NM}$ is the incompressibility coefficient which is directly related to the curvature of the EOS, $K_{\rm NM} = 9\rho_0^2\frac{\partial^2 E_0}{\partial\rho^2}|_{\rho_0}$. Similarly, the EOS of asymmetric NM, with proton density $\rho_{\rm p}$ and neutron density $\rho_{\rm n}$, can be approximated by

$$E[\rho_{\rm p},\rho_{\rm n}] = E_0[\rho] + E_{\rm sym}[\rho]\left(\frac{\rho_{\rm n}-\rho_{\rm p}}{\rho}\right)^2, \tag{26}$$

TABLE III. Properties of symmetric nuclear matter at nuclear saturation density ρ_0 (fm^3) associated with the Skyrme interactions of table. Also shown are the total binding energy per nucleon E/A (MeV), isoscalar effective mass m^*/m, incompressibility modulus $K_{\rm NM}$ (MeV), the coefficients related to the symmetry energy density J (MeV), L (MeV), and $K_{\rm sym}$ (MeV), and the enhancement factor of the EWSR of the IVGDR, κ.

	E/A	ρ_0	m^*/m	$K_{\rm NM}$	J	L	$K_{\rm sym}$	κ
SGII	15.59	0.159	0.79	215.0	26.80	37.63	−145.90	0.49
KDE0	16.11	0.161	0.72	228.8	33.00	45.22	−144.78	0.30
KDE0v1	16.23	0.165	0.74	227.5	34.58	54.70	−127.12	0.23
SKM*	15.78	0.160	0.79	216.7	30.03	45.78	−155.94	0.53
SK255	16.33	0.157	0.80	255.0	37.40	95.00	−58.33	0.54
SkI3	15.96	0.158	0.58	258.1	34.80	100.52	73.04	0.25
SkI4	15.92	0.160	0.65	247.9	29.50	60.39	−40.56	0.25
SkI5	15.83	0.156	0.58	255.7	36.70	129.33	159.57	0.25
SV-bas	15.90	0.160	0.90	234.0	30.00	45.21	−221.75	0.40
SV-min	15.91	0.161	0.95	222.0	30.01	44.76	−156.57	0.08
SV-m56-O	15.81	0.157	0.56	254.6	27.00	49.96	−45.04	0.60
SV-m64-O	15.82	0.159	0.64	241.5	27.01	30.63	−144.76	0.60
SLy4	15.97	0.160	0.70	229.9	32.00	45.96	−119.73	0.25
SLy5	15.98	0.160	0.70	229.9	32.03	48.27	−112.76	0.25
SLy6	15.92	0.159	0.69	229.8	31.96	47.44	−112.71	0.25
SkMP	15.56	0.157	0.65	230.9	29.88	70.31	−49.82	0.71
SkP	15.93	0.162	1.00	200.8	32.98	45.21	−266.60	0.30
SkO’	15.75	0.160	0.90	222.3	31.95	68.93	−78.82	0.15

TABLE IV. Pearson correlation coefficients among the various NM properties and spin-orbit strength W_0 with the centroid energies of the isoscalar $T0$ giant resonances of multipolarities $L = 0$–3.

					m^*/m	$K_{\rm NM}$	J	L	$K_{\rm sym}$	κ	$W_0(x_{\rm w}=1)$
$L0$	$T0$	Ca	40	$E_{\rm CEN}$	−0.75	0.95	0.07	0.56	0.78	0.20	0.00
$L0$	$T0$	Ca	48	$E_{\rm CEN}$	−0.79	0.88	0.02	0.56	0.80	0.24	0.30
$L0$	$T0$			$\Delta E_{\rm CEN}$	−0.31	0.07	−0.11	0.16	0.25	0.18	0.73
$L1$	$T0$	Ca	40	$E_{\rm CEN}$	−0.84	0.74	−0.20	0.30	0.64	0.47	0.24
$L1$	$T0$	Ca	48	$E_{\rm CEN}$	−0.89	0.71	−0.11	0.25	0.62	0.25	0.46
$L1$	$T0$			$\Delta E_{\rm CEN}$	−0.30	0.14	0.11	−0.02	0.12	−0.28	0.54
$L2$	$T0$	Ca	40	$E_{\rm CEN}$	−0.97	0.81	−0.03	0.40	0.76	0.22	0.48
$L2$	$T0$	Ca	48	$E_{\rm CEN}$	−0.97	0.75	−0.06	0.36	0.74	0.22	0.57
$L2$	$T0$			$\Delta E_{\rm CEN}$	−0.20	−0.26	−0.20	−0.18	−0.02	0.00	0.52
$L3$	$T0$	Ca	40	$E_{\rm CEN}$	−0.96	0.80	−0.05	0.35	0.73	0.23	0.41
$L3$	$T0$	Ca	48	$E_{\rm CEN}$	−0.98	0.73	−0.08	0.33	0.72	0.27	0.59
$L3$	$T0$			$\Delta E_{\rm CEN}$	−0.11	−0.25	−0.13	−0.07	−0.01	0.16	0.56

where $E_{\rm sym}[\rho]$ is the symmetry energy at matter density ρ, approximated as

$$E_{\rm sym}[\rho] = J + \frac{1}{3}{\rm L}\left(\frac{\rho-\rho_0}{\rho_0}\right) + \frac{1}{18}K_{\rm sym}\left(\frac{\rho-\rho_0}{\rho_0}\right)^2, \tag{27}$$

where $J = E_{\rm sym}[\rho_0]$ is the symmetry energy at saturation density ρ_0, $L = 3\rho_0 \frac{\partial E_{\rm sym}}{\partial \rho}|_{\rho_0}$, and $K_{\rm sym} = 9\rho_0 \frac{\partial^2 E_{\rm sym}}{\partial \rho^2}|_{\rho_0}$.

Table III contains the values of the physical quantities of symmetric nuclear matter associated with these Skyrme interactions: the binding energy per nucleon E/A, the saturation matter density ρ_0, the effective mass m^*/m, the incompressibility coefficient of SNM, $K_{\rm NM}$, the coefficients associated with the symmetry energy density J, L, and $K_{\rm sym}$ at saturation density ρ_0 [Eq. (27)] and κ, the NM value of the enhancement factor of the EWSR of the IVGDR, Eq. (22), obtained from Eq. (23) with using the NM saturation matter density.

III. RESULTS

We now present results of our fully self-consistent HF-based RPA calculations of the strength functions and centroid energies of isoscalar and isovector giant resonances of multipolarities $L = 0$–3 in ^{40}Ca and ^{48}Ca, obtained for 18 widely used Skyrme-type interactions shown in Table I: SGII [23], KDE0 [24], KDE0v1 [24], SKM* [25], SK255 [26], SkI3 [40], SkI4 [40], SkI5 [40], SV-bas [41], SV-min [41], SV-m56-O [42], SV-m64-O [42], SLy4 [43], SLy5 [43], SLy6 [43], SkMP [44], SkP [45], and SkO' [46]. These interactions are associated with the ranges of NM properties (see Table III): $E/A = 15.56$–16.33 MeV, $\rho_0 = 0.156$–0.165 fm^{-3}, $K_{\rm NM} = 201$–258 MeV, $J = 26.80$–37.40 MeV, $L = 31$–129 MeV, $K_{\rm sym} = -267 - 160$ MeV, $m^*/m = 0.56$–1.00, and $\kappa = 0.08$–0.71.

In Figs. 1–4 we display the HF-based RPA results (solid lines) for the distribution of the energy-weighted strength normalized to one [ES(E)/EWSR] for the isoscalar and isovector giant resonances of multipolarities $L = 0$–3 in ^{40}Ca and ^{48}Ca, obtained using the KDE0 [24] interaction that is representative of the strength distributions for the rest of the interactions. For the purpose of comparison with experiment a Lorenzian smearing of a 3 MeV width was used in the calculation. The experimental data [19,21] are shown as histograms.

To investigate the sensitivity of the energies of the giant resonances in ^{40}Ca and ^{48}Ca to NM properties (Table III) we calculated the Pearson correlation coefficients (a measure of linear correlation) between the centroid energies $E_{\rm CEN}$,

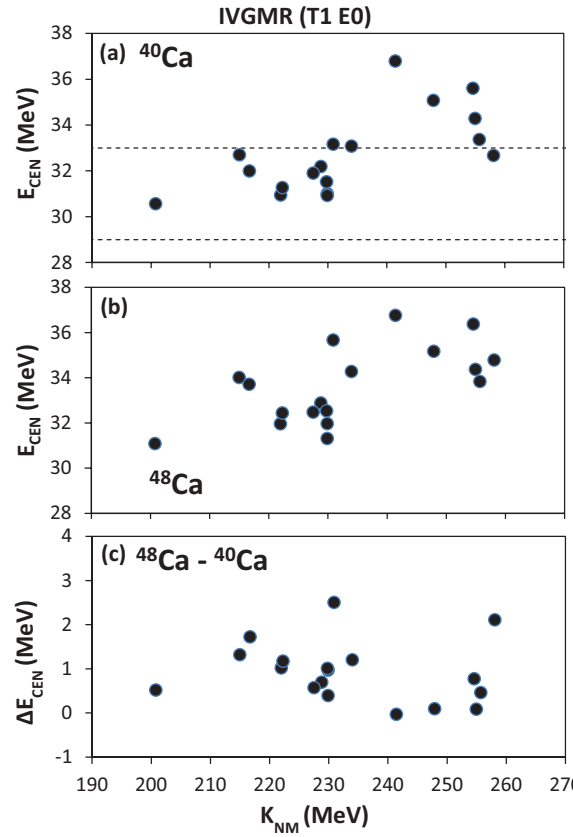

FIG. 13. (Color online) Same as Fig. 7 except for the IVGMR as a function of $K_{\rm NM}$. The experimental data are taken from Ref. [10,47].

Eq. (19), and the properties of NM. We used a small smearing width (0.05 MeV) to insure accuracy for $E_{\rm CEN}$. For a proper comparison with experiment, we used the experimental excitation energy ranges in determining the centroid energies. We use the excitation energy range of 9.5–40 MeV [19,21] for the ISGMR and the ISGQR and the range of 20–40 MeV [19,21] for the ISGDR. For the ISGOR we use the appropriate excitation energy range of 20–60 MeV. We use the excitation energy range of 0–60 MeV for the IVGMR [10,47], the range of 0–40 MeV for the IVGDR [48–50], the range of 9–60 MeV for the IVGQR [51], and the range of 25–60 MeV for the IVGOR (see also Figs. 1–4).

A. ISGMR

In Fig. 5 we compare the experimental data [19,21] of the ISGMR centroid energies of ^{40}Ca (a), ^{48}Ca (b), and the energy difference, $\Delta E_{\rm CEN} = E_{\rm CEN}(^{48}{\rm Ca}) - E_{\rm CEN}(^{40}{\rm Ca})$, between ^{48}Ca and ^{40}Ca (c) with the results of fully self-consistent HF-based RPA calculations (solid circles), obtained using the 18 Skyrme interactions of Table I. The results obtained with violation of self-consistency, by neglecting the Coulomb and the spin-orbit particle-hole interactions in the RPA calculations, are shown in Fig. 5(d). The calculated values are plotted as a function of $K_{\rm NM}$. The experimental values of $E_{\rm CEN} = 19.18 \pm 0.37$ MeV for ^{40}Ca, $E_{\rm CEN} = 19.88 \pm 0.16$ MeV for ^{48}Ca [19,21], and their differences are shown in Fig. 5 as the regions between the dashed lines. A very strong correlation between $E_{\rm CEN}$ of ^{40}Ca and $E_{\rm CEN}$ of ^{48}Ca can be seen with $K_{\rm NM}$. This is expected, because the ISGMR centroid energy is very sensitive to the value of $K_{\rm NM}$ [1,3,8]. The ISGMR centroid energies for ^{40}Ca are all higher than the experimental value 19.18 ± 0.37 MeV. The ^{48}Ca ISGMR centroid energies are more consistent with the experimental value 19.88 ± 0.16 MeV. While the experimental data show that the ISGMR in ^{40}Ca lies at lower energy than in ^{48}Ca, 17 of the Skyrme interactions (Table I) show the ISGMR in ^{40}Ca at a higher energy than in ^{48}Ca, while the 18th interaction (SkI3) shows them at essentially the same energy in ^{40}Ca and ^{48}Ca. For not fully self-consistent RPA calculations, the results for some interactions leads to spurious agreement with the experimental data for the ^{48}Ca–^{40}Ca energy difference as can be seen in Fig. 5(d). We also found a medium correlation between the ISGMR energies and the effective mass m^*/m, which is a reflection of the strong correlation between $K_{\rm NM}$ and m^*/m seen in Fig. 6 (see also Ref. [8]). Figure 6 also shows the correlation of the saturation symmetric NM density ρ_0 and the symmetry energy coefficient J with $K_{\rm NM}$.

To investigate the dependence of the energy difference $\Delta E_{\rm CEN} = E_{\rm CEN}(^{48}{\rm Ca}) - E_{\rm CEN}(^{40}{\rm Ca})$ between the ISGMR in ^{48}Ca and in ^{40}Ca on the symmetry energy density, Fig. 7 shows the results of our fully self-consistent HF-based RPA calculations (solid circles), using the Skyrme interactions (Table I) having nuclear matter symmetry energy coefficient $J = 26.80$–36.7 MeV. No correlation is found between $\Delta E_{\rm CEN}$ and J. Similar results were obtained for L, $K_{\rm sym}$, and $K_{\rm NM}$,

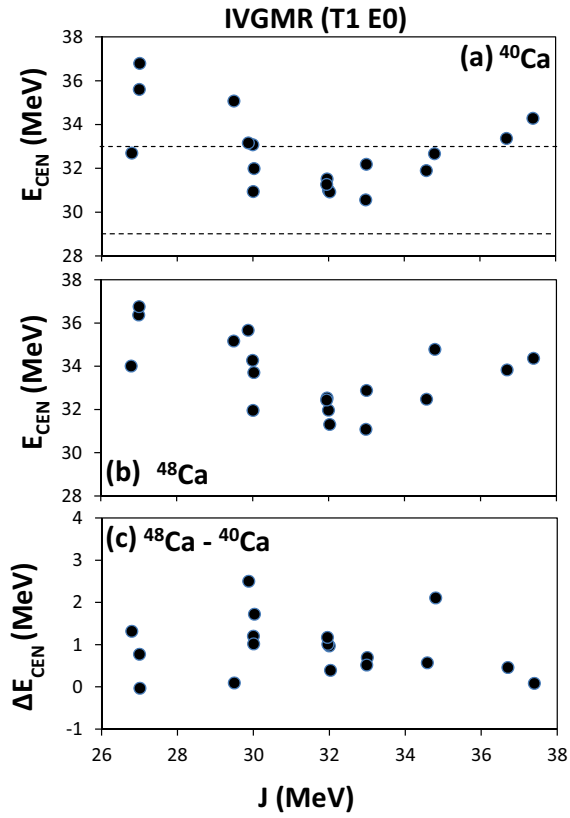

FIG. 14. (Color online) Same as Fig. 13 except as a function of J.

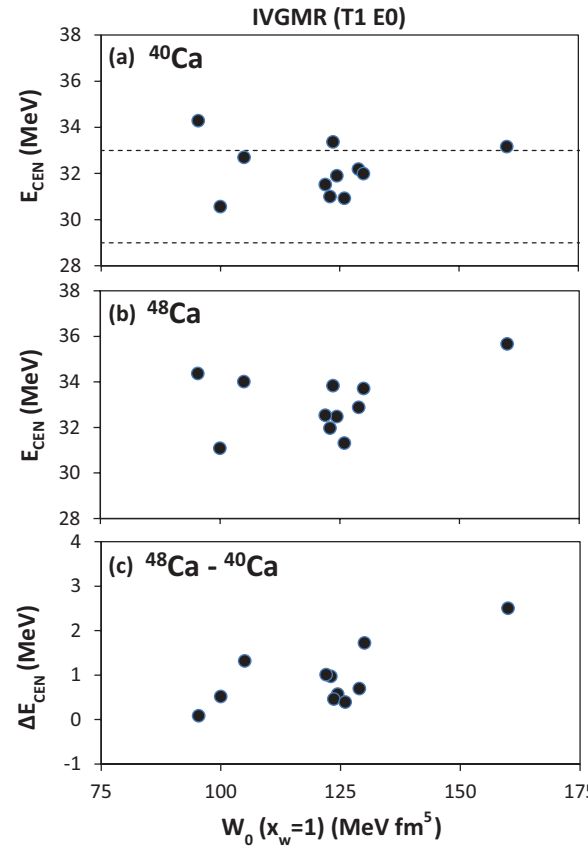

FIG. 15. (Color online) Same as Fig. 13 except as a function of W_0.

which can be easily understood as a reflection of the correlation of $K_{\rm sym}$, J, and $K_{\rm NM}$ with L shown in Fig. 8.

Figure 9 shows the correlation of the ISGMR centroid energies with W_0, the strength of the spin-orbit interaction. There is a positive strong correlation between the ^{48}Ca – ^{40}Ca energy difference and W_0. Similar results were obtained for the ISGDR, ISGQR, and ISGOR.

B. ISGDR

In Fig. 10 the results of the self-consistent HF-based RPA calculations (solid circles) for the ISGDR centroid energies of ^{40}Ca (a), ^{48}Ca (b), and the ^{48}Ca – ^{40}Ca energy difference (c), are compared with the experimental data [19,21]. The experimental values of $E_{\rm CEN} = 23.36 \pm 0.70$ MeV for ^{40}Ca, $E_{\rm CEN} = 27.30 \pm 0.15$ MeV for ^{48}Ca and their difference are shown in Fig. 10 as the regions between the dashed lines. The HF-RPA energies, obtained for the interactions of Table I, are plotted as a function of $K_{\rm NM}$. For all the Skyrme interactions of Table I, the calculated ISGDR centroid energies are higher than the experimental values by 1.5–6 MeV and the calculated ^{48}Ca – ^{40}Ca energy difference, although positive, are smaller than the experimental value. We note that the experimental results for the fraction of the EWSR for the ISGDR in ^{48}Ca and ^{40}Ca are $137 \pm 20\%$ and $62 \pm 20\%$ [19,21], respectively, compared to the calculated values of 100%. Therefore, the comparison between the ISGDR in ^{48}Ca and ^{40}Ca might be misleading because only $62 \pm 20\%$ of the EWSR of the ISGDR in ^{40}Ca was found experimentally. A strong correlation is also found between the ISGDR energy of ^{40}Ca with both $K_{\rm NM}$ and m^*/m and similarly for ^{48}Ca.

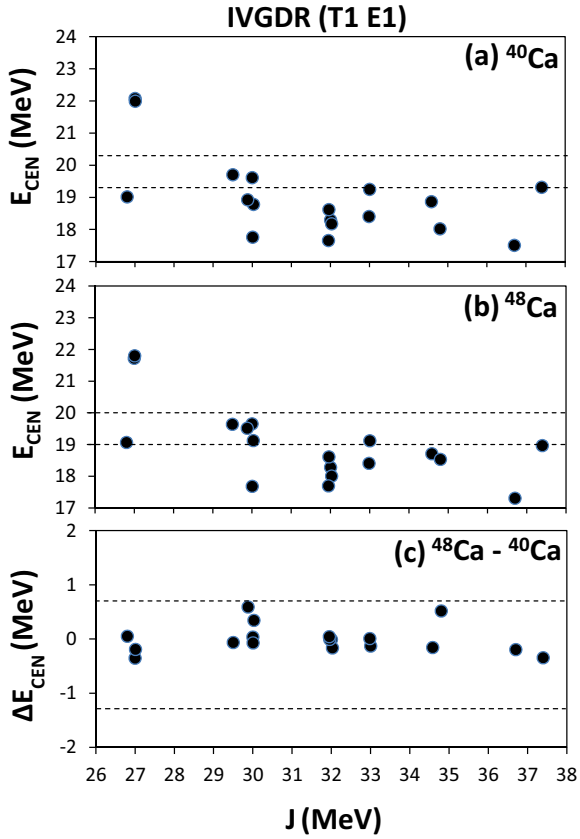

FIG. 16. (Color online) Same as Fig. 7 except for the IVGDR. The experimental data are taken from Refs. [48–50].

C. ISGQR

Figure 11 shows, as a function of m^*/m, our HF-based RPA results (solid circles) of the ISGQR centroid energies $E_{\rm CEN}$, of ^{40}Ca (a), ^{48}Ca (b), and the ^{48}Ca–^{40}Ca energy difference (c), obtained using the Skyrme-type interactions of Table I. The experimental values of $E_{\rm CEN} = 17.84 \pm 0.43$ MeV for ^{40}Ca [19], $E_{\rm CEN} = 18.61 \pm 0.24$ MeV for ^{48}Ca [21] and their difference are shown in Fig. 11 as the regions between the dashed lines. As seen in Fig. 11, a very strong correlation exists between the ISGQR energy of ^{40}Ca with m^*/m and similarly for ^{48}Ca. We find that interactions having $m^*/m =$ 0.65–0.8 reproduce the experimental data of the ISGQR.

D. ISGOR

Figure 12 shows our HF-based RPA results (solid circles) of the ISGOR centroid energies $E_{\rm CEN}$, of ^{40}Ca (a), ^{48}Ca (b), and the ^{48}Ca – ^{40}Ca energy difference (c), using the Skyrme-type interactions of Table I. A very strong correlation exists between the ISGOR energy of ^{40}Ca and ^{48}Ca with m^*/m as can be seen in Fig. 12. Using the result that interactions having $m^*/m =$ 0.65–0.8 reproduce the experimental data of the ISGQR we can predict the values of the $E_{\rm CEN}$ of the ISGOR in ^{40}Ca and ^{48}Ca to be in the region of 30–34 MeV.

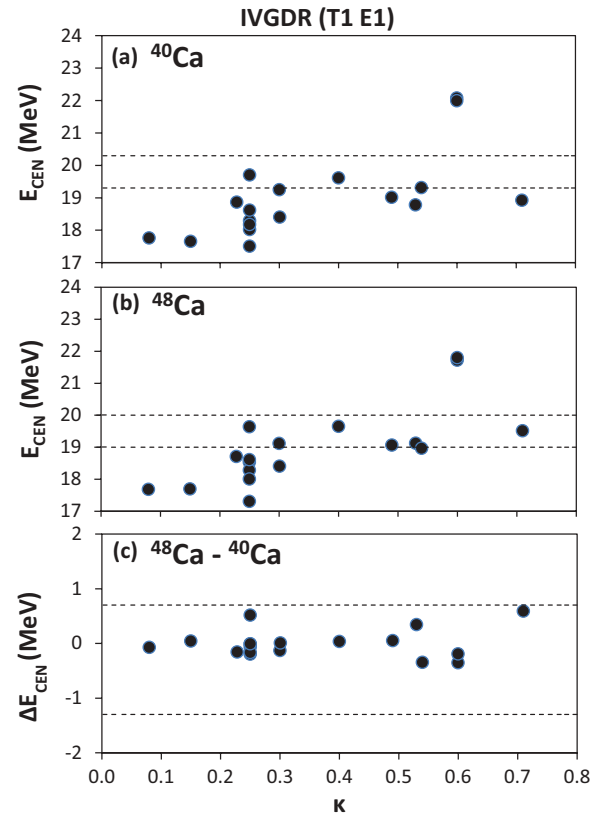

FIG. 17. (Color online) Same as Fig. 16 except as a function of κ.

For completeness we present in Table IV the values of the Pearson correlation coefficients among the various NM properties and spin-orbit strength W_0 with the centroid energies of the isoscalar (T 0) giant resonances of multipolarities $L = 0$–3. We find no correlations or very weak correlations between the ^{48}Ca – ^{40}Ca centroid energy differences of the isoscalar giant resonances with the coefficients J, L, or $K_{\rm sym}$, associated with the density dependence of the symmetry energy and a strong correlation with the value of W_0.

E. IVGMR

For the IVGMR, an isovector compression mode, we show the HF-RPA results (solid circles), obtained using the Skyrme interactions of Table I, for the centroid energies $E_{\rm CEN}$ of ^{40}Ca (a), ^{48}Ca (b), and the ^{48}Ca – ^{40}Ca energy difference (c) as a function of $K_{\rm NM}$ in Fig. 13 and as a function of J in Fig. 14. The experimental value of $E_{\rm CEN} = 31 \pm 2$ MeV for ^{40}Ca [10,46] is shown as the region between the dashed lines. We find a medium correlation between $E_{\rm CEN}$ of the IVGMR with $K_{\rm NM}$ and a weak correlation with J, L, or $K_{\rm sym.}$ It can be seen from Fig. 14 that a stronger correlation between the IVGMR energy and $K_{\rm NM}$ is obtained for a fixed value of J (at 27 and 30 MeV).

Figure 15 shows the IVGMR centroid energies as a function of W_0, the strength of the spin-orbit interaction. A strong positive correlation between the ^{48}Ca – ^{40}Ca energy difference and the value of W_0 is seen. Similar results were obtained for the IVGDR and the IVGQR.

F. IVGDR

Figure 16 shows, as a function of J, our HF-based RPA results (solid circles) of the IVGDR centroid energies $E_{\rm CEN}$ of ^{40}Ca (a), ^{48}Ca (b), and the ^{48}Ca – ^{40}Ca energy difference (c), obtained using the Skyrme-type interactions of Table I. The experimental values of $E_{\rm CEN} = 19.8 \pm 0.5$ MeV for ^{40}Ca, $E_{\rm CEN} = 19.5 \pm 0.5$ MeV for ^{48}Ca [48–50] and their differences are shown in Fig. 16 as the regions between the dashed lines. Weak correlations can be seen between $E_{\rm CEN}$ of ^{40}Ca and $E_{\rm CEN}$ of ^{48}Ca with J. Similar results were obtained for L and $K_{\rm sym}$.

Figure 17 shows the IVGDR centroid energies as a function of κ, the enhancement factor in the EWSR of the IVGDR. Strong positive correlations between the IVGDR centroid energy of ^{40}Ca and of ^{48}Ca with κ are seen in the figure.

G. IVGQR

Figure 18 shows, as a function of m^*/m, the HF-based RPA results (solid circles) of the IVGQR centroid energies $E_{\rm CEN}$ of ^{40}Ca (a), ^{48}Ca (b), and the ^{48}Ca – ^{40}Ca energy difference (c), obtained using the Skyrme-type interactions of Table I. The

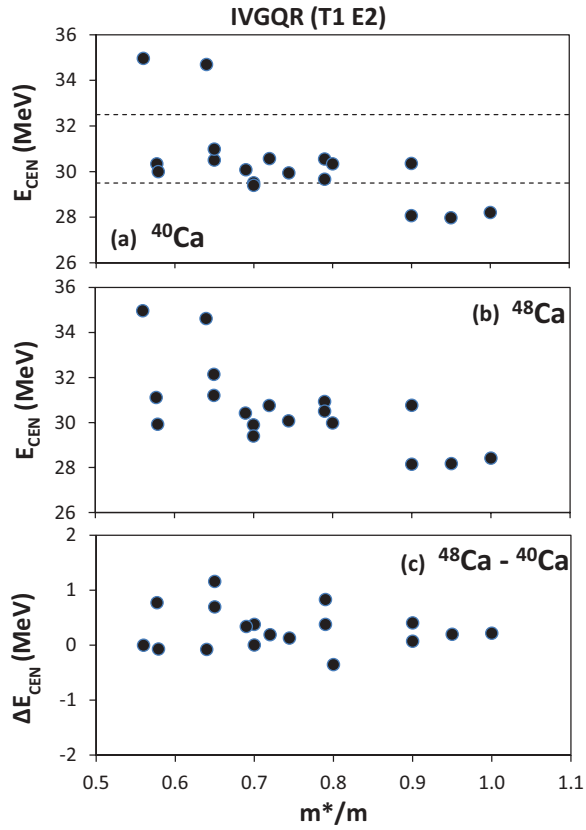

FIG. 18. (Color online) Same as Fig. 11 except for the IVGQR. The experimental data are taken from Ref. [51].

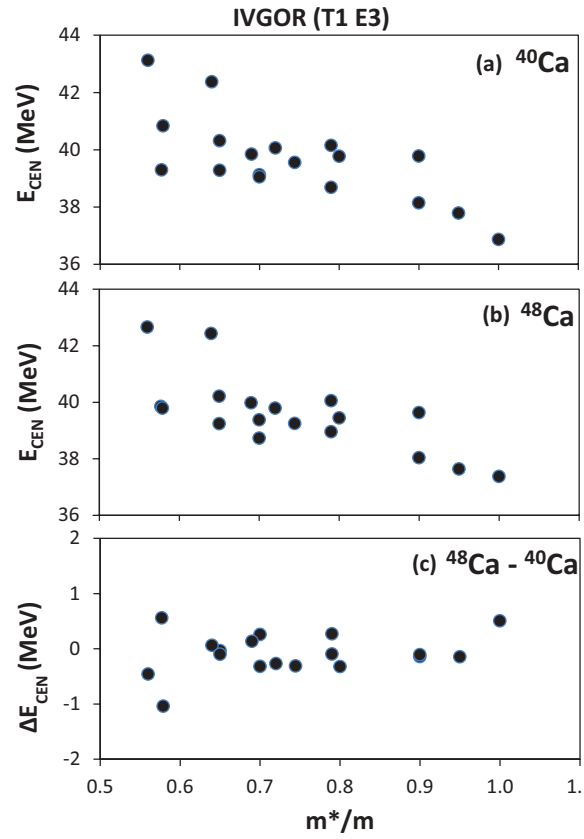

FIG. 19. (Color online) Same as Fig. 18 except for the IVGOR.

TABLE V. Pearson correlation coefficients among the various NM properties and spin-orbit strength W_0 with the centroid energies of the isovector $T1$ giant resonances of multipolarities $L = 0$–3.

					m^*/m	$K_{\rm NM}$	J	L	$K_{\rm sym}$	κ	$W_0(x_{\rm w}=1)$
$L0$	$T1$	Ca	40	$E_{\rm CEN}$	−0.54	0.66	−0.33	0.10	0.31	0.61	0.01
$L0$	$T1$	Ca	48	$E_{\rm CEN}$	−0.64	0.62	−0.35	0.17	0.40	0.74	0.36
$L0$	$T1$			$\Delta E_{\rm CEN}$	−0.25	−0.10	−0.06	0.16	0.22	0.31	0.70
$L1$	$T1$	Ca	40	$E_{\rm CEN}$	−0.34	0.31	−0.58	−0.40	−0.17	0.66	−0.07
$L1$	$T1$	Ca	48	$E_{\rm CEN}$	−0.36	0.28	−0.63	−0.40	−0.17	0.73	0.23
$L1$	$T1$			$\Delta E_{\rm CEN}$	−0.01	−0.22	−0.09	0.09	0.07	0.14	0.67
$L2$	$T1$	Ca	40	$E_{\rm CEN}$	−0.64	0.52	−0.47	−0.14	0.16	0.68	0.43
$L2$	$T1$	Ca	48	$E_{\rm CEN}$	−0.70	0.49	−0.50	−0.14	0.19	0.73	0.66
$L2$	$T1$			$\Delta E_{\rm CEN}$	−0.33	−0.10	−0.18	0.02	0.14	0.27	0.71
$L3$	$T1$	Ca	40	$E_{\rm CEN}$	−0.73	0.61	−0.33	0.04	0.36	0.60	0.37
$L3$	$T1$	Ca	48	$E_{\rm CEN}$	−0.71	0.56	−0.43	−0.07	0.26	0.65	0.42
$L3$	$T1$			$\Delta E_{\rm CEN}$	0.34	−0.42	−0.21	−0.41	−0.47	−0.08	−0.11

experimental data of $E_{\rm CEN} = 31 \pm 1.5$ MeV for ^{40}Ca [51] is shown as the region between the dashed lines. Medium correlations between m^*/m and $E_{\rm CEN}$ of ^{40}Ca and $E_{\rm CEN}$ of ^{48}Ca can be seen in Fig. 18.

H. IVGOR

Figure 19 shows, as a function of m^*/m, the HF-based RPA results (solid circles) of the IVGOR centroid energies $E_{\rm CEN}$ of ^{40}Ca (a), ^{48}Ca (b), and the ^{48}Ca – ^{40}Ca energy difference (c), obtained using the Skyrme-type interactions of Table I. Medium correlations between m^*/m and $E_{\rm CEN}$ of ^{40}Ca and $E_{\rm CEN}$ of ^{48}Ca can be seen in Fig. 19.

For completeness we present in Table V the values of the Pearson correlation coefficients among the various NM properties and spin-orbit strength W_0 with the centroid energies of the isovector ($T1$) giant resonances of multipolarities $L = 0$–3.

As shown in Table V, only weak correlations exist between the $E_{\rm CEN}$ of the isovector giant resonances of ^{40}Ca or ^{48}Ca with J, L, and $K_{\rm sym}$. A strong correlation is found between the ^{48}Ca – ^{40}Ca centroid energy difference of the IVGMRs, IVDGRs, and IVGQRs with W_0. We also note the strong correlation between the $E_{\rm CEN}$ of the IVGDR and the value of κ.

IV. CONCLUSIONS

We have presented results of our fully self-consistent HF-RPA calculations using 18 commonly employed Skyrme-type interactions of Table I, for the centroid energies of isoscalar and isovector giant resonances of multipolarities $L = 0$–3 in ^{40}Ca and ^{48}Ca and compared with available experimental data. We have investigated and discussed the sensitivity of the $E_{\rm CEN}$ of the giant resonances to various properties of NM. In particular, we point out that

(i) For all the 18 Skyrme interactions used in our HF-based RPA calculations (Table I) the ^{48}Ca –^{40}Ca centroid energy differences of the ISGMR are smaller than the experimental data. For 17 of the Skyrme interactions used in our HF-based RPA calculations the ^{40}Ca ISGMR lies above that for ^{48}Ca. The 18th interaction (SkI3) predicts the ISGMR in about the same location in both nuclei.

(ii) We have demonstrated the very strong to strong correlations of the $E_{\rm CEN}$ of the compression modes, the ISGMR and the ISGDR, with the NM incompressibility coefficient $K_{\rm NM}$ and noted that the sensitivity of $E_{\rm CEN}$ to the effective mass is a reflection of the correlation between m^*/m and $K_{\rm NM}$, existing in the Skyrme interactions used in our calculations.

(iii) For all the adopted Skyrme interactions, the calculated centroid energies of the ISGDR in ^{40}Ca and ^{48}Ca are consistently higher than the experimental data (by about 1.5–6 MeV).

(iv) We have demonstrated the very strong correlation of $E_{\rm CEN}$ of the ISGQR and the ISGOR with m^*/m. We have found that an agreement with the experimental data for $E_{\rm CEN}$ of the ISGQR in ^{40}Ca and ^{48}Ca is obtained for a value of the effective mass in the range of $m^*/m = 0.65$–0.8. Using this result we can predict that the values of the $E_{\rm CEN}$ of the ISGOR in ^{40}Ca and ^{48}Ca should be in the region of 30–34 MeV.

(v) We find no correlations or very weak correlations between the ^{48}Ca–^{40}Ca centroid energy differences of the isoscalar giant resonances of multipolarities $L = 0$–3 with the coefficients J, L, or $K_{\rm sym}$, associated with the density dependence of the symmetry energy. Similar results were found for the isovector giant resonances of multipolarities $L = 0$–3.

(vi) We find positive strong correlations between the ^{48}Ca – ^{40}Ca centroid energy differences ($\Delta E_{\rm CEN}$) of the isoscalar and isovector giant resonances with W_0.

(vii) For the IVGMR, the isovector compression mode, we find a medium correlation with $K_{\rm NM}$ and a weak correlation with J, L, or $K_{\rm sym.}$

(viii) We find a weak correlation between the energies of the IVGDR of ^{40}Ca (and ^{48}Ca) and the quantities associated with the density dependence of the symmetry energy.

(ix) We find a strong correlation between the energies of the IVGDR of ^{40}Ca (and ^{48}Ca) and the value of κ.
(x) For the IVGQR and IVGOR we find a strong correlation between $E_{\rm CEN}$ and m^*/m.

The disagreement between the HF-RPA results and the experimental data for the centroid energies of the ISGMR and ISGDR in ^{40}Ca and ^{48}Ca remain unsolved problems which call for possible extension of the EDF used in the work, microscopic calculations of the excitation cross sections of giant resonances [38,52], and/or going beyond the HF-RPA theory. [53]

ACKNOWLEDGMENTS

This work was supported in part by US Department of Energy under Grant No. DOE-FG03-93ER40773.

[1] A. Bohr and B. M. Mottelson, *Nuclear Structure II* (Benjamin, New York, 1975).
[2] P. Ring and P. Schuck, *The Nuclear Many-Body Problem* (Springer, New York-Heidelberg-Berlin, 1980).
[3] S. Shlomo, V. M. Kolomietz, and G. Colo, Eur. Phys. J. A **30**, 23 (2006), and references therein.
[4] N. K. Glendenning, Phys. Rev. C **37**, 2733 (1988).
[5] J. M. Lattimer and M. Prakash, Phys. Rep. **442**, 109 (2007).
[6] W. D. Myers and W. J. Swiatecki, Phys. Rev. C **57**, 3020 (1998).
[7] L. Satpathy, V. S. U. Maheshwari, and R. C. Nayak, Phys. Rep. **319**, 85 (1999).
[8] J. P. Blaizot, Phys. Rep. **64**, 171 (1980).
[9] H. Krivine, J. Treiner, and O. Bohigas, Nucl. Phys. A **336**, 155 (1984).
[10] E. Lipparini and S. Stringari, Phys. Rep. **175**, 103 (1989).
[11] J. Treiner, H. Krivine, and O. Bohigas, Nucl. Phys. A **371**, 253 (1981).
[12] D. H. Youngblood, P. Bogucki, J. D. Bronson, U. Garg, Y.-W. Lui, and C. M. Rozsa, Phys. Rev. C **23**, 1997 (1981).
[13] B. K. Jennings and A. D. Jackson, Phys. Rep. **66**, 141 (1980).
[14] S. Shlomo and D. H. Youngblood, Phys. Rev. C **47**, 529 (1993), and references therein.
[15] J. M. Pearson, N. Chamel, and S. Goriely, Phys. Rev. C **82**, 037301 (2010).
[16] T. H. R. Skyrme, Phil. Mag. **1**, 1043 (1956).
[17] T. H. R. Skyrme, Nucl. Phys. **9**, 615 (1959).
[18] D. Vautherin and D. M. Brink, Phys. Rev. C **5**, 626 (1972).
[19] Y.-W. Lui, D. H. Youngblood, S. Shlomo, X. Chen, Y. Tokimoto, Krishichayan, M. Anders, and J. Button, Phys. Rev. C **83**, 044327 (2011).
[20] D. H. Youngblood, Y.-W. Lui, H. L. Clark, Y. Tokimoto, and B. John, Phys. Rev. C **68**, 057303 (2003).
[21] D. H. Youngblood, Y.-W. Lui, and H. L. Clark, Phys. Rev. C **63**, 067301 (2001).
[22] D. H. Youngblood, Y.-W. Lui, and H. L. Clark, Phys. Rev. C **55**, 2811 (1997).
[23] Nguyen Van Giai and H. Sagawa, Phys. Lett. B **106**, 379 (1981).
[24] B. K. Agrawal, S. Shlomo, and V. K. Au, Phys. Rev. C **72**, 014310 (2005).
[25] J. Bartel, P. Quentin, M. Brack, C. Guet, and H. B. Hakansson, Nucl. Phys. A **382**, 79 (1986).
[26] B. K. Agrawal, S. Shlomo, and V. KimAu, Phys. Rev. C **68**, 031304 (2003).
[27] S. Shlomo and G. Bertsch, Nucl. Phys. A **243**, 507 (1975).
[28] P.-G. Reinhardt, Ann. Phys. (Leipzig) **1**, 632 (1992).
[29] T. Nakatsukasa, T. Inakura, and K. Yabana, Phys. Rev. C **76**, 024318 (2007).
[30] E. Chabanat, P. Bonche, P. Haensel, J. Meyer, and R. Schaeffer, Nucl. Phys. A **627**, 710 (1997).
[31] W. Kohn, Rev. Mod. Phys. **71**, 1253 (1999).
[32] S. Shlomo, Rep. Prog. Phys. **41**, 957 (1978).
[33] M. Bender, P. H. Heenen, and P.-G. Reinhard, Rev. Mod. Phys. **75**, 121 (2003).
[34] M. Dutta, O. Lourenco, J. S. Sa Martins, A. Delfino, J. R. Stone, and P. D. Stevenson, Phys. Rev. C **85**, 035201 (2012).
[35] S. Shlomo and W. G. Love, Physica Scripta **26**, 280 (1982).
[36] Tapas Sil, S. Shlomo, B. K. Agrawal, and P.-G. Reinhard, Phys. Rev. C **73**, 034316 (2006).
[37] V. O. Nesterenko, J. Kvasil, and P.-G. Reinhard, Phys. Rev. C **66**, 044307 (2002).
[38] S. Shlomo and A. I. Sanzhur, Phys. Rev. C **65**, 044310 (2002).
[39] B. K. Agrawal, S. Shlomo, and A. I. Sanzhur, Phys. Rev. C **67**, 034314 (2003).
[40] P.-G. Reinhard and H. Flocard, Nucl. Phys. A **587**, 467 (1995).
[41] P. Klupfel, P.-G. Reinhard, T. J. Burvenich, and J. A. Maruhn, Phys. Rev. C **79**, 034310 (2009).
[42] N. Lyutorovich, V. I. Tselyaev, J. Speth, S. Krewald, F. Grummer, and P.-G. Reinhard, Phys. Rev. Lett. **109**, 092502 (2012).
[43] E. Chabanat, P. Bonche, P. Haensel, J. Meyer, and R. Schaeffer, Nucl. Phys. A **635**, 231 (1998).
[44] L. Bennour, P.-H. Heenen, P. Bonche, J. Dobaczewski, and H. Flocard, Phys. Rev. C **40**, 2834 (1989).
[45] J. Dobaczewski, H. Flocard, and J. Treiner, Nucl. Phys. A **422**, 103 (1984).
[46] P.-G. Reinhard, D. J. Dean, W. Nazarewicz, J. Dobaczewski, J. A. Maruhn, and M. R. Strayer, Phys. Rev. C **60**, 014316 (1999).
[47] A. Erell, J. Alster, J. Lichtenstadt, M. A. Moinester, J. D. Bowman, M. D. Cooper, F. Irom, H. S. Matis, E. Piasetzky, and U. Sennhauser, Phys. Rev. C **34**, 1822 (1986).
[48] P. Gleissl, M. Brack, J. Meyer, and P. Quentin, Ann. Phys. **197**, 205 (1990).
[49] A. Veyssière, H. Beil, R. Bergère, P. Carlos, A. Leprêtre, and A. De Miniac, Nucl. Phys. A **277**, 513 (1974).
[50] G. J. O'keefe, M. N. Thompson, Y. I. Assafiri, R. E. Pywell, and K. Shoda, Nucl. Phys. A **469**, 239 (1987).
[51] D. A. Sims *et al.*, Phys. Rev. C **55**, 1288 (1997).
[52] A. Kolomiets, O. Pochivalov, and S. Shlomo, Phys. Rev. C **61**, 034312 (2000).
[53] S. Kamerdzhiev, J. Speth, and G. Tertchny, Eur. Phys. J. A **7**, 483 (2000); Phys. Reports **393**, 1 (2004).